Soft Matter

Accepted Manuscript

ROYAL SOCIETY OF CHEMISTRY

www.rsc.org/softmatter

How Dimensionality Changes Anomalous Behavior and Melting Scenario of Core-Softened Potential System

D.E. Dudalov,[1] Yu.D. Fomin,[1,2] E.N. Tsiok,[1] and V.N. Ryzhov[1,2]

[1] *Institute for High Pressure Physics RAS, 142190 Kaluzhskoe shosse, 14, Troitsk, Moscow, Russia*
[2] *Moscow Institute of Physics and Technology, 141700 Moscow, Russia*

(Dated: April 11, 2014)

We present a computer simulation study of a phase diagram and anomalous behavior of two-dimensional ($2D$) and three dimensional ($3D$) classical particles repelling each other through an isotropic core-softened potential. As in the analogous three-dimensional case, in $2D$ a reentrant-melting transition occurs upon compression for not too high pressures, along with a spectrum of thermodynamic and dynamic anomalies in the fluid phase. However, in two dimensions the order of the region of anomalous diffusion and the region of structural anomaly is inverted in comparison with the $3D$ case, where there exists a waterlike sequence of anomalies, and has a silicalike sequence. In the low density part of the $2D$ phase diagram melting is a continuous two-stage transition, with an intermediate hexatic phase. All available evidence supports the Kosterlitz-Thouless-Halperin-Nelson-Young (KTHNY) scenario for this melting transition. On the other hand, at high density part of the phase diagram one first-order transition takes place.

PACS numbers: 61.20.Gy, 61.20.Ne, 64.60.Kw

INTRODUCTION

In recent years, a growing attention has been paid to investigation of confined fluids in relation with the different fields of modern technology such as fabrication of nanomaterials, nanotribology, adhesion, and nanotechnology [1, 2]. That confined fluids microscopically relax and flow with different characteristic time scales than bulk liquids is hardly surprising. Confining boundaries bias the spatial distribution of the constituent molecules and the ways by which those molecules can dynamically rearrange. These effects play important roles in the thermodynamics of the confined systems. The fundamental question is how the properties of a system change as the dimensionality changes from three dimensions ($3D$) to two dimensions ($2D$).

The main goal of the paper is to compare the behavior of the system with the core-softened potential in three (3D) and two (2D) dimensions. This comparison can give some qualitative hints for understanding the role of the confinement in the behavior of the systems with core-softened potentials, which are used for the qualitative description of the behavior of anomalous liquids like water. In three dimensions the properties of the systems with the core-softened potentials are well studied (see, for example, Refs. [3–17, 20]). There are two fundamental aspects which can be different with the change of the dimensionality. First of all, it is the possible change of the behavior of the thermodynamic and dynamic anomalies. In the second place, the question is whether the melting scenario in $2D$ can be different from the melting in $3D$. Both these problems are closely related because in $3D$ the anomalous regions are located near the maximum on the melting curve of the systems [3–6, 8–10, 16]. It is widely believed now, that in $3D$ the anomalies are related with the Widom line [8, 21–24], which is located in this region [8, 21, 24]. It seems that the similar behavior may exist in $2D$ [16]. One can expect that the difference in the spatial distribution of the particles in $2D$ and $3D$ cases can lead to the considerable change of the anomalous behavior. The second important reason for this change is the considerable growth of the density fluctuations in $2D$. The fluctuations can change the melting scenario of the system from the ordinary first order transition to two continuous transitions (see below). The diffusion above the continuous melting transition line can be radically different than in the case of the first order transition. As a result, the anomalous behavior can qualitatively change in comparison with the $3D$ system. In this work we discuss these changes on the basis of the same core-softened potential, introduced in our previous publications, properties of which are well known in $3D$ [3–8].

It is well known that some liquids demonstrate anomalous behavior in some regions of thermodynamic parameters. The most common and well known example is water. The water phase diagrams have regions where a thermal expansion coefficient is negative (density anomaly), self-diffusivity increases upon compression (diffusion anomaly), and the structural order of the system decreases with increasing pressure (structural anomaly). Later on it was discovered that many other substances also demonstrate similar behavior. Some typical examples are silica, silicon, phosphorus, and many others. It is reasonable to relate this kind of behavior to the orientational anisotropy of the potentials, however, a number of studies demonstrate waterlike anomalies in fluids that interact through spherically symmetric core-softened potentials with two length scales. A lot of different core-softened potentials were introduced (see, for

example, reviews [9, 10]). However, it should be noted that in general the existence of two length scales is not enough to mark the occurrence of the anomalies. For example, for the models studied in Ref. [16, 17] it was shown that the existence of two distinct repulsive length scales is not a necessary condition for the occurrence of anomalous phase behavior.

As found in experiments [18] and simulations [19, 20], the water anomalies have a well-defined sequence: the regions where these anomalies take place form nested domains in the density-temperature [19] (or pressure-temperature [20]) planes: the density anomaly region is located inside the diffusion anomaly domain, and both of these anomalous regions are located inside a broader structurally anomalous region.

However, in other anomalous systems, the sequence of anomalies may be different. For example, in computer simulation of the system with the Van Beest-Kramer-Van Santen (BKS) potential, the hierarchy of anomalies in silica is different compared to water [25]. In this case, the diffusion anomaly region contains the structural anomalous region which, in turn, incorporates the density anomaly region. It is widely believed that in the core-softened systems the hierarchy of anomalies is of the water-like type. However, recently it was shown that the order of the region of anomalous diffusion and the regions of density and structural anomalies may be inverted depending on the parameters of the potential and may have the silicalike or some other sequences [5, 6, 8].

In the case of the melting transition, the most interesting topics concern the existence of the specific $2D$ phase, hexatic phase, that interpolates between the fluid and ordered solid phases, and the dependence of the nature of $2D$ phase transition on the character of the interparticle interaction. In $3D$, systems melt through the first-order transition due to the third-order term in the Landau expansion. However, in $2D$ the singular fluctuations of the order parameter (dislocations and disclinations) may cause the qualitative differences between $2D$ and $3D$ behavior of matter [26–29].

Despite the long history of investigations, the melting transition of most materials in $2D$ is not well understood, because theories explaining the transition on a microscopic scale are not available. Furthermore, the mechanism of melting depends on the details of the interactions between the particles forming the crystal lattice. In their pioneering works, Halperin, Nelson, and Young [30], using the Kosterlitz-Thouless ideas [31], proposed the scenario of two-dimensional melting which is fundamentally different from the melting scenario of conventional three-dimensional systems. It has been shown that the transition between a crystal and an isotropic liquid can occur by means of two continuous transitions which correspond to dissociation of bound dislocation and disclination pairs, respectively. The low-temperature solid phase is characterized by quasi-long-range translational order and long-range bond-orientational order. Dislocations unbinding at some temperature T_m leads to a phase with short-range translational order, but with quasi-long-range bond-orientational order. This intermediate phase is called a hexatic phase. Paired disclinations in the hexatic phase ultimately unbind themselves, driving a second transition at a higher temperature T_i into an isotropic liquid.

This theory has strong support from experiments with electrons on helium [32] and computer simulations of the 2D electron systems [33]. An experimental confirmation for the KTHNY theory for crystal melting in $2D$ has been found in the colloidal model system with repulsive magnetic dipole-dipole interaction [34–36]. However, a conventional first-order transition between a two-dimensional solid and an isotropic liquid is also a possibility (see, for example, [37–40]).

It should be noted that the KTHNY theory is phenomenological and seems universal. It is not clear from this theory whether the melting scenario depends on the shape of an intermolecular potential. Actually, the natural way to analyze this dependence is to use computer simulations. However, simulations are not reliable enough in the case of two-dimensional melting: it is interesting to note that the similar simulation methods have led to contradictory conclusions even when applied to the same systems [16, 41–50]. The problems are understandable since correlation times and lengths (translational and orientational) can be extremely long near the phase transition. A lot of efforts were made on computational studies of two-dimensional melting of hard-core potential systems including hard disks or Lennard-Jones potentials. Simulation results on these systems tend to favor a first-order transition scenario for melting, although some conflicting results also exist [41–47]. In spite of all these efforts, a satisfactory answer has not been obtained yet for one of the most important questions in two-dimensional melting, which is as follows: what condition determines the existence of a hexatic phase and the nature of the melting transition? It seems natural to relate this behavior with the range and the softness of the potential [16, 49, 50].

In this work, we present a simulation study of phase diagram and anomalous behavior in the purely repulsive core-softened system introduced in our previous publications [3–8]. The general form of the potential is written as

$$U(r) = \varepsilon \left(\frac{\sigma}{r}\right)^{14} + \frac{1}{2}\varepsilon \left(1 - \tanh(k_1\{r - \sigma_1\})\right). \qquad (1)$$

Here $k_1 = 10.0$, and $\sigma_1 = 1.35$. In the remainder of this paper we use the dimensionless quantities, which in $2D$ have the form: $\tilde{\mathbf{r}} \equiv \mathbf{r}/\sigma$, $\tilde{P} \equiv P\sigma^2/\varepsilon$, $\tilde{V} \equiv V/N\sigma^2 \equiv 1/\tilde{\rho}, \tilde{T} \equiv k_B T/\varepsilon$. Since we will use only these reduced variables, the tildes will be omitted. The potential (1) is plotted in Fig. 1.

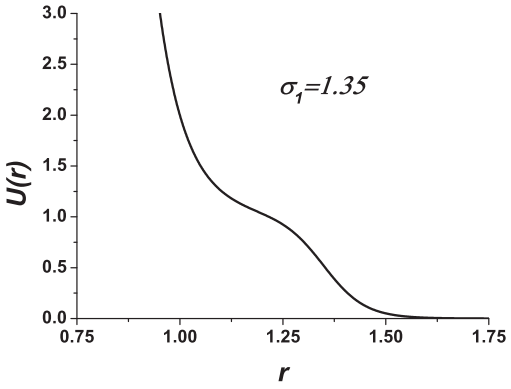

FIG. 1: The potential (1) with $\sigma_1 = 1.35$.

In $3D$, particles interacting through a core-softened potential exhibit reentrant melting, a maximum melting temperature, superfragile glass behavior, and anomalies similar to the ones found in water and silica [3–8].

PHASE DIAGRAM AND ANOMALOUS BEHAVIOR

Here we present the anomalous regions for the $3D$ and $2D$ systems.

The first anomaly mentioned in the Introduction is density anomaly. It means that density increases upon heating or that the thermal expansion coefficient becomes negative. Using the thermodynamic relation $(\partial P/\partial T)_V = \alpha_P/K_T$, where α_P is a thermal expansion coefficient and K_T is the isothermal compressibility and taking into account that K_T is always positive and finite for systems in equilibrium not at a critical point, we conclude that density anomaly corresponds to minimum of the pressure dependence on temperature along an isochor. This is the most convenient indicator of density anomaly in computer simulation.

If we consider a simple liquid (for, example, Lennard-Jones liquid), and trace the diffusion along an isotherm we find that the diffusion decreases with increasing density. This observation is intuitively clear - if density increases the free volume decreases and the particles have less freedom to move. However, some substances have a region in density - temperature plane where diffusion grows under increase of the density. This is called an anomalous diffusion region which reflects the contradiction of this behavior with the free volume picture described above. This means that diffusion anomaly involves more complex mechanisms which will be discussed below.

The last anomaly we discuss here is structural anomaly. The local order is related to excess entropy of the liquid which is defined as the difference between the entropy and the ideal gas entropy at the same (ρ, T) point: $S_{ex} = S - S_{id}$. In normal liquid excess entropy is monotonically decaying function of density along an isotherm while in anomalous liquids it demonstrates increasing in some region. This allows to define the boundaries of structural anomaly at given temperature as minimum and maximum of excess entropy.

In order to find the line of the first order melting transition, we carry out the free energy calculations for different phases and construct a common tangent to them. For our purely repulsive potentials we computed the free energy of the liquid by integrating the equation of state along an isotherm [51]: $\frac{F(\rho)-F_{id}(\rho)}{Nk_BT} = \frac{1}{k_BT}\int_0^\rho \frac{P(\rho')-\rho' k_BT}{\rho'^2}d\rho'$. Free energies of different crystal phases were determined by the Monte Carlo simulations with the method of coupling to the Einstein crystal [51]. To improve the statistics (and to check for internal consistency) the free energy of the solid was computed at many dozens of different state points and fitted to multinomial function. The fitting function we used is $a_{p,q}T^pV^q$, where T and $V = 1/\rho$ are the temperature and specific volume and powers p and q are related through $p + q \leq N$. The value N we used for the most of calculations is 5.

In this case the excess entropy can be computed via $S_{ex} = \frac{U-F_{ex}}{Nk_BT}$, where U is the internal energy [51]. The total entropy is $S = S_{ex}+S_{id}$, where the ideal gas entropy is $\frac{S_{id}}{Nk_B} = \frac{3}{2}\ln(T) - \ln(\rho) + \ln(\frac{(2\pi mk_B)^{3/2}e^{5/2}}{h^3})$.

Fig. 2 shows the $3D$ phase diagrams that we obtain from the free-energy calculations for $\sigma_1 = 1.35$. In fact, the phase diagrams for $\sigma_1 = 1.15, 1.35, 1.55, 1.8$ were already reported in Refs. [3, 4].

Fig. 2(a) shows the $3D$ phase diagram of the system with $\sigma_1 = 1.35$ in the $\rho - T$ plane. There is a clear maximum in the melting curve at low densities. The phase diagram consists of two Face Centered Cubic (FCC) domains corresponding to close packing of the small and large spheres separated by a sequence of structural phase transitions (including Face Centered Tetragonal (FCT), Simple Cubic (SC) and Simple Hexagonal (SH) structures). This phase diagram was discussed in detail in our previous publications [3, 4]. It is important to note that there is a region of the phase diagram where we have not found any stable crystal phase. The results of Ref. [3, 7] suggest that a glass transition occurs in this region. The apparent glass-transition temperature is above the melting point of the low-density FCC and FCT phases. If, indeed, no other crystalline phases are stable in this region, the "glassy" phase that we observe would be thermodynamically stable. This is rather unusual for one-component liquids. In simulations, glassy behavior is usually observed in metastable mixtures, where crystal nucleation is kinetically suppressed. One could argue that, in the glassy region, the present system behaves like a "quasi-binary" mixture of spheres with diameters

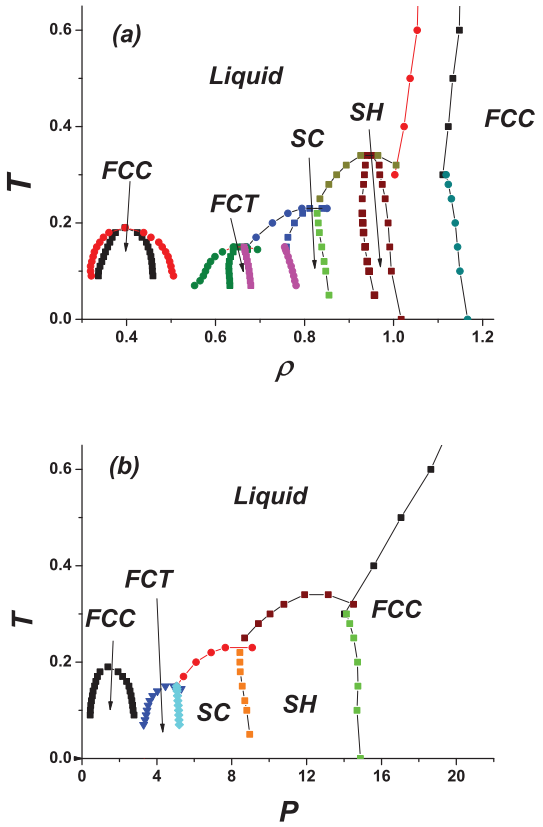

FIG. 2: (Color online) Phase diagram of the $3D$ system of particles interacting through the potential (1) with $\sigma_1 = 1.35$ in $\rho - T$ (a) and $P - T$ (b) planes.

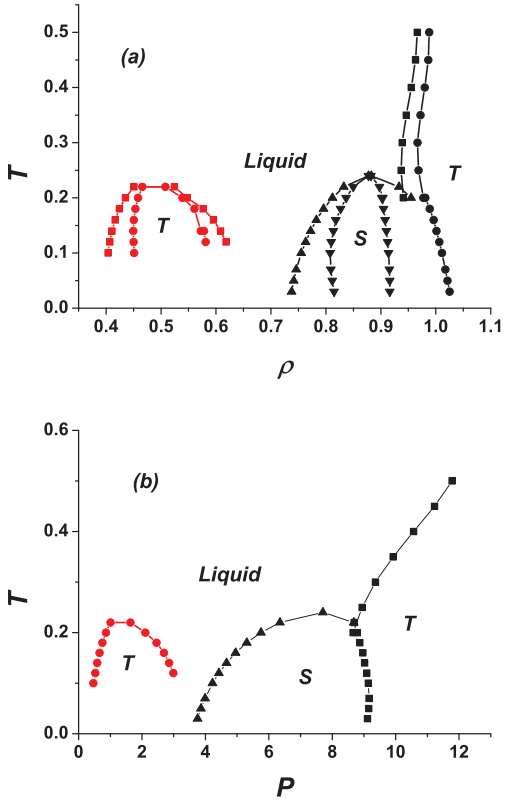

FIG. 3: (Color online) (a) Phase diagram of the $2D$ system with the potential (1) in $\rho - T$ plane, where the Triangular (T) and Square (S) phases are shown. (b) Phase diagram of the same system in the $P - T$ plane.

σ and σ_1 [3, 7]. The glassy behavior in the reentrant liquid disappears at higher temperatures.

We plot in Fig. 3 the phase diagram of $2D$ system in $\rho - T$ and $P - T$ coordinates. There is a clear maximum in the melting curve at low densities. The phase diagram consists of two triangular crystal domains (T) corresponding to close packing of the small and large disks separated by a structural phase transition and square lattice (S). It is important to note that there is a region of the phase diagram where we have not found any stable crystal phase at the temperatures accessible in our simulations. The results of $3D$ simulations [3, 7] suggest that a glass transition can occur in this region.

The phase diagrams in $2D$ and $3D$ are qualitatively similar. They consist in two structures which are close packed in corresponding dimensions: FCC in $3D$ and triangular in $2D$, between which there are some other phases which depend on the parameters of the potential and dimensionality. These structures correspond to the crystalline phases of small spheres (at high densities) and large spheres (at low densities). The qualitative shape of the phase diagrams is determined by the existence of two scales in the potential [3]. Despite an obvious qualitative similarity of the phase diagrams in two and three dimension, the melting scenarios of these systems are drastically different, as it will be shown in the next section.

Figs. 4 (a)-(c) show the diffusion coefficient, pressure and excess entropy for the $3D$ system with $\sigma_1 = 1.35$. One can see that all three anomalies take place in the system. It is also evident that structural anomaly is more stable than the diffusion one since it disappears at higher temperatures.

Fig. 5 places the regions of the anomalies on the phase diagram of the $3D$ system (see Fig. 2). In Fig. 5 we show the low density part of the phase diagram with the FCC and FCT (Face Centered Tetragonal) phases. One can see that all three anomalous regions appear after the maximum on the low-density FCC crystal part. It is widely believed now, that in $3D$ the anomalies are related with the Widom line [8, 21–24], which is located in this region, however, the discussion of this issue is far from the main scope of the article [8, 21, 24]. Recently it was shown that there are strict thermodynamic arguments that the density anomaly must be inside the region of the structural anomaly (see, for example, [5, 8] and references therein), however, the location of the range of the

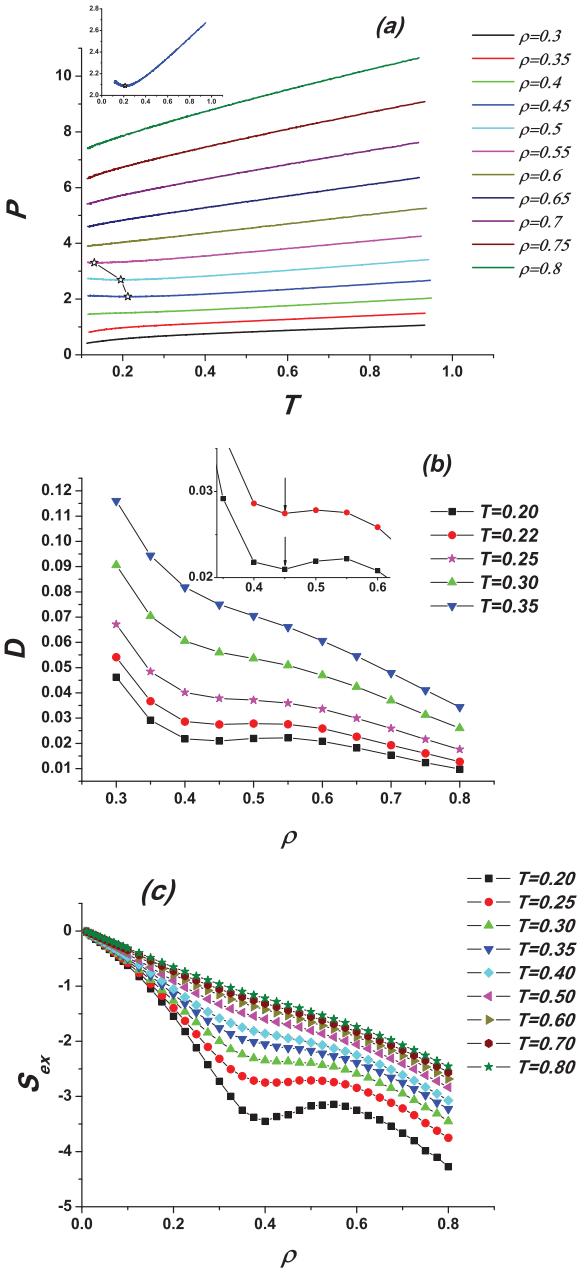

FIG. 4: (Color online) The $3D$ system with $\sigma_1 = 1.35$. (a) Pressure along a set of isochors as a function of temperature. Stars mark the minima on isochores which correspond to the density anomaly; (b) Diffusion coefficient along a set of isotherms as a function of density. Diffusion anomaly corresponds to the region where the diffusion coefficient is increasing with increasing density. Arrows mark the positions of the diffusion coefficient minima; (c) Excess entropy along a set of isotherms as a function of density. At low temperatures there are regions where the excess entropy is increasing with increasing density (structural anomaly)

.

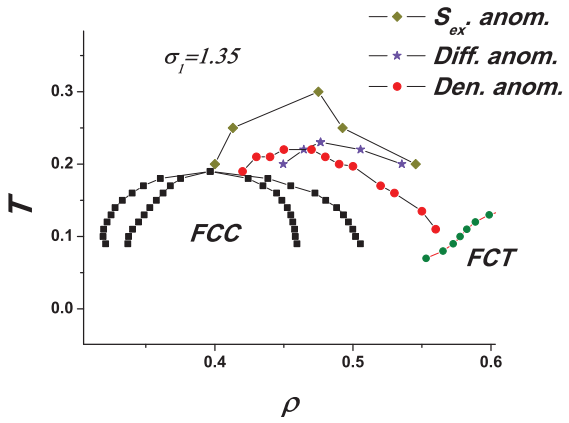

FIG. 5: (Color online) Location of anomalous regions at the low density part of the phase diagram of the $3D$ system with $\sigma_1 = 1.35$, where Face Centered Cubic (FCC) and Face Centered Tetragonal (FCT) phases are shown.

diffusion anomaly can be anywhere in $(T-\rho)$ plane. Our calculations show that there is a range of the densities where the regions of the anomalies form the waterlike sequence [19]: the diffusion anomaly region is under the structural anomaly and the density anomaly is under the diffusion anomaly. Unfortunately, this is not true for the whole range of the anomalous behavior of the diffusion.

In the previous publications [53–57], where the core-softened potentials, different from (1), were discussed, it was shown that some of the mentioned above anomalies also exist in $2D$, however, the order of the sequence of the anomalies has not been investigated. In $2D$, for the potential (1) we also found the anomalies (see Fig. 6(a-c)), however, the order of the region of anomalous diffusion and the region of structural anomaly is inverted in comparison with the $3D$ case and has silicalike sequence (see Fig. 7) [6, 8, 25]. This fact shows that the dynamics of $2D$ liquids is really different from the dynamics of the corresponding $3D$ system.

It should be noted, that in $2D$ the similar sequence of anomalies was found in Ref. [16] for extremely soft potential, however, the authors of Ref. [16] did not compare the $2D$ and $3D$ cases.

TWO-DIMENSIONAL MELTING OF CORE-SOFTENED SYSTEM

As it was discussed before [28, 29], there are two characteristic temperatures for the melting transition in $2D$: the dislocation unbinding temperature T_m and the first-order transition temperature T_{MF} [28, 29] which can be obtained from the double-tangent construction for the free energies of liquid and solid phases. There are two possibilities [28, 29]: 1: $T_m < T_{MF}$. In this case the system melts via two continuous transitions of the

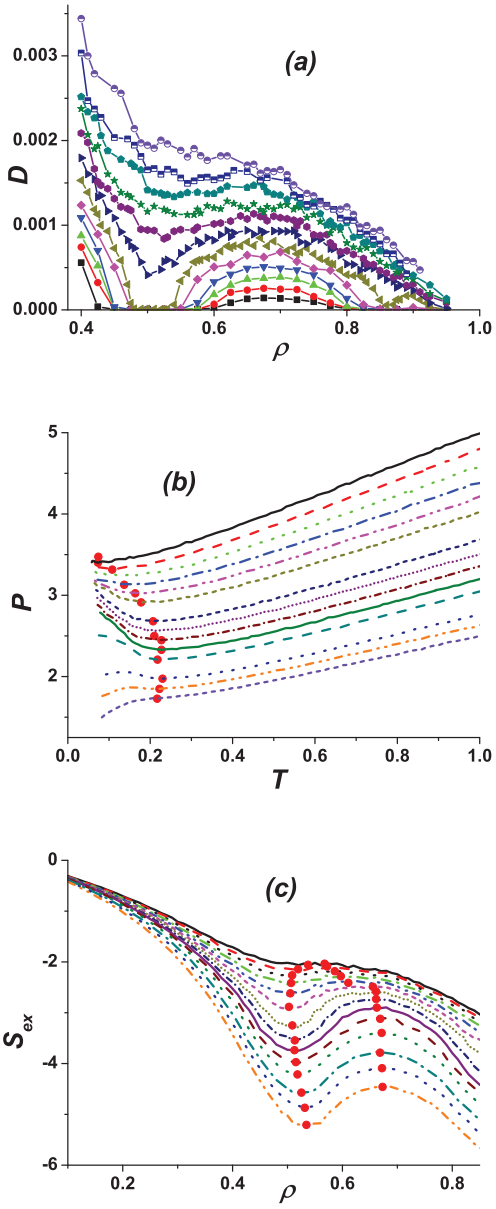

FIG. 6: (Color online) In $2D$: (a) Diffusion coefficient along a set of isotherms as a function of density. Results are for temperatures $T = 0.1$, 0.12, 0.14, 0.18, 0.20, 0.22, 0.24, 0.26, 0.28, 0.30, 0.32 from bottom up. At low temperatures, there are regions where the diffusion coefficient is increasing with increasing density (diffusion anomaly); (b) pressure along a set of isochors as a function of temperature. The lines correspond to densities $\rho = 0.51$, 0.52, 0.53, 0.55, 0.56, 0.57, 0.58, 0.59, 0.61, 0.62, 0.63, 0.64, 0.65, 0.66 from bottom to top. Minima on isochores correspond to the density anomaly and are marked by the red points; (c) excess entropy S_{ex} along a set of isotherms as a function of density. $S_{ex} = S - S_{id}$ is equal to the difference between the total S and ideal gas S_{id} entropies. Results are for temperatures $T = 0.03$, 0.05, 0.07, 0.10, 0.12, 0.14, 0.16, 0.18, 0.20, 0.22, 0.24, 0.26, 0.28, 0.30 from bottom up. At low temperatures, there are regions where the excess entropy is increasing with increasing density (structural anomaly). Red points correspond to the minima (left branch) and maxima (right branch) of S_{ex}.

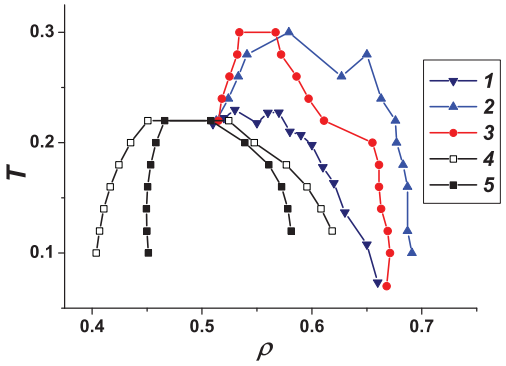

FIG. 7: (Color online) The boundaries of anomaly regions in $2D$: 1). isobaric ρ maxima (density anomaly); 2). isothermal D minima and maxima (left and right blue triangles); 3). isothermal S_{ex} minima and maxima(left and right red balls); 4). and 5). the borders of the low-density triangle phase. The silicalike [6, 8, 25] order of anomalies takes place: the diffusion anomaly region contains the structurally anomalous region which, in turn, incorporates the density anomaly region.

Kosterlitz-Thouless type with the unbinding of dislocation pairs. 2: $T_m > T_{MF}$. The system melts via a first-order transition because of the existence of third-order terms in the Landau expansion as in the ordinary three-dimensional case [28, 29]. The phase diagram corresponding to T_{MF}, gives the limit of the thermodynamic stability of the solid phase. In order to conclude whether the melting occurs through the KTHNY scenario, the additional analysis is necessary.

We simulate the system in NVT and NVE ensembles using the molecular dynamics (LAMMPS package [52]). The number of particles in the simulation varied between 3200 and 102400. In order to find the transition points we carry out the free energy calculations for different phases and construct a common tangent to them. In our work we consider the purely repulsive potential (1). In this case there is no liquid-gas transition, and the Helmholtz free energy of the liquid can be calculated by integrating the equation of state along an isotherm [51]:

$$\frac{F(\rho) - F_{id}(\rho)}{Nk_BT} = \frac{1}{k_BT}\int_0^{\rho} \frac{P(\rho') - \rho' k_B T}{\rho'^2} d\rho'. \qquad (2)$$

. Free energies of different crystal phases were determined by the method of coupling to the Einstein crystal [51]. The phase diagram calculated in this way corresponds to the first-order transitions scenario. It should be noted, that if the potential has the attractive part, the gas-liquid phase transition can exist. In this case one cannot use the simple formula (2), and instead of, it is necessary to choose the thermodynamic path around the critical point of the liquid-gas phase transition in order to calculate the free energy of the liquid phase.

To disentangle first-order from continuous melting, we

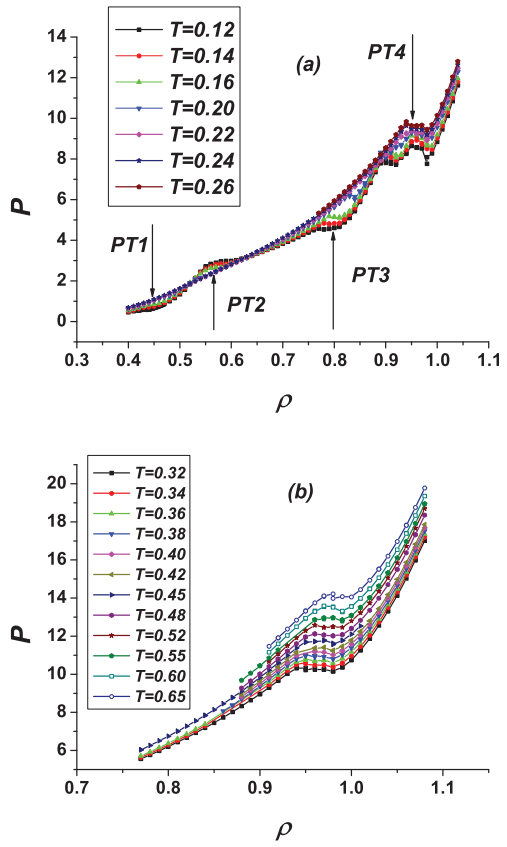

FIG. 8: (Color online) The low-temperature (a) and high-temperature (b) sets of isotherms. The arrows mark the phase transitions (compare with Fig. 3(a)).

used the criteria described in the Ref. [47]. In Fig. 8 we present the low-temperature (Fig. 8(a)) and high-temperature (Fig. 8(b)) sets of isotherms. One can see that at low temperatures there are four regions on the isotherms corresponding to the phase transitions (see Fig. 8(a)), the low density ones being smooth as in the case of liquid-hexatic-solid transition [47] and the high densities part containing the Van der Waals loops characteristic of the first order phase transition. At high temperatures (see Fig. 8(b)) there is only one liquid-triangular lattice first-order transition. From Fig. 8 one can guess that the melting of the low-density and high-density parts of the phase diagram occurs with different scenarios: at low densities the KTHNY scenario is probable, while the high density phase melts through the first-order phase transition. As we are going to show in the following, the intermediate region between the low density triangular solid and the (normal) fluid can be qualified as hexatic.

To confirm this guess, let us consider two different order parameters (OP), which are separately sensitive to the overall translational and orientational order, with their respective correlation functions. The translational OP is taken to be

$$\psi_T = \frac{1}{N}\left\langle \left| \sum_i e^{i\mathbf{G}\mathbf{r}_i} \right| \right\rangle, \tag{3}$$

where the sum is over the particle labels and $\mathbf{G}$ is any first shell reciprocal-lattice vector of the crystal. From its very definition, it follows that ψ_T is sizeable only in a solid that is oriented in a way consistent with the length and direction of $\mathbf{G}$. Hence, ψ_T is only measured on heating, where memory of the original crystal orientation is preserved as long as the system is large and remains solid. A sharp drop of ψ_T signals the melting of the solid into a fluid, be it hexatic or normal.

At regular intervals during the simulation, we used of the Voronoi construction in order to identify the $n_c(i)$ nearest neighbors (NN) of each particle i, together with the orientation θ_{NN} of each neighbor bond with respect to a reference axis. Whence, the orientational OP follows as

$$\psi_6 = \frac{1}{N}\left\langle \left| \sum_i \frac{1}{n_c(i)} \sum_{NN(i)} e^{6i\theta_{NN}} \right| \right\rangle = \frac{1}{N}\left\langle \left| \sum_i \Psi_6(\mathbf{r}_i) \right| \right\rangle. \tag{4}$$

The corresponding susceptibility

$$\chi_6 = \frac{1}{N}\left\langle \left| \sum_i \Psi_6(\mathbf{r}_i) \right|^2 \right\rangle - N\psi_6^2, \tag{5}$$

shows a distinct peak whose location is an unambiguous estimate of the transition point.

The local bond-angular OP $\Psi_6(\mathbf{r}_i)$ enters the definition of the orientational correlation function (OCF):

$$G_6(r) = \rho^{-2}\left\langle {\sum_{i,j}}' \delta(\mathbf{r}_i - \mathbf{R})\delta(\mathbf{r}_i - \mathbf{R}')\Psi_6(\mathbf{r}_i)\Psi_6^*(\mathbf{r}_j) \right\rangle, \tag{6}$$

where the prime over the sum excludes $i = j$ and $r = |\mathbf{R} - \mathbf{R}'|$. The KTHNY theory predicts an algebraic $r^{-\eta(T)}$ large-distance decay of the OCF in the hexatic phase, which should be contrasted with the exponential asymptotic vanishing of angular correlations in a normal fluid. Another prediction of the theory is $\eta = 1/4$ at the hexatic-to-normal fluid transition point [30].

In Fig. 9(a), we represent the orientational order parameter (OOP) as a function of density for a set of temperatures. We see, that at the low density part of the phase diagram OOP behaves smoothly while at high densities one can see the abrupt change of OOP. This kind of behavior suggests again that the melting at low densities is continuous in accordance with the KTHNY scenario, and at high densities melting transition is of the first order. In Fig. 9(b), the corresponding susceptibility is shown as a function of density for several temperatures. The precise behavior of the susceptibility at

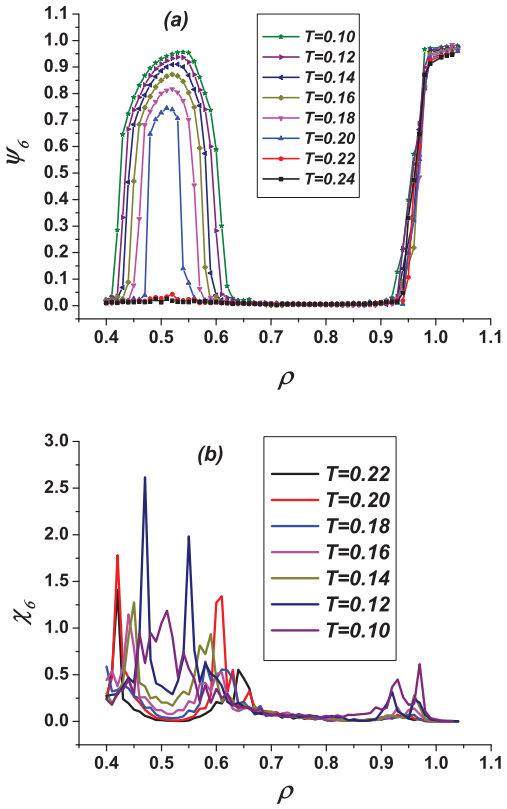

FIG. 9: (Color online) (a) Orientational order parameter as a function of density for different temperatures; (b) The corresponding susceptibility χ_6 as a function of density for different temperatures.

the transition lines depends on the assumed melting scenario [30, 42]. If the transition is of first order, the susceptibility should assume finite values at the transition densities, and interpolate linearly between them. The KTHNY theory, on the other hand, predicts that the bond-orientational susceptibility diverges as the transition density is approached from the fluid [30]. One can see in Fig. 9(b), that at low densities, χ_6 demonstrates the sharp peaks characteristic for the continuous transition, while at high densities the peaks are much smaller, as in the case of the first-order phase transition.

In Fig. 10, we plot the translational and orientational OPs for $\rho = 0.45, 0.48, 0.56, 0.58$ as a function of temperature (an analogous behavior was observed for all the other densities). We see that ψ_T vanishes at a slightly smaller temperature than ψ_6, which implies that the hexatic phase is confined to a narrow T interval. The results shown in Fig. 10 were obtained from the molecular dynamic simulations of 7200 particles. It is necessary to note, that in the case of the conventional first-order phase transition, the density change at the melting line maximum is equal to zero. For the density close to the maximum on the low density part of the phase diagram

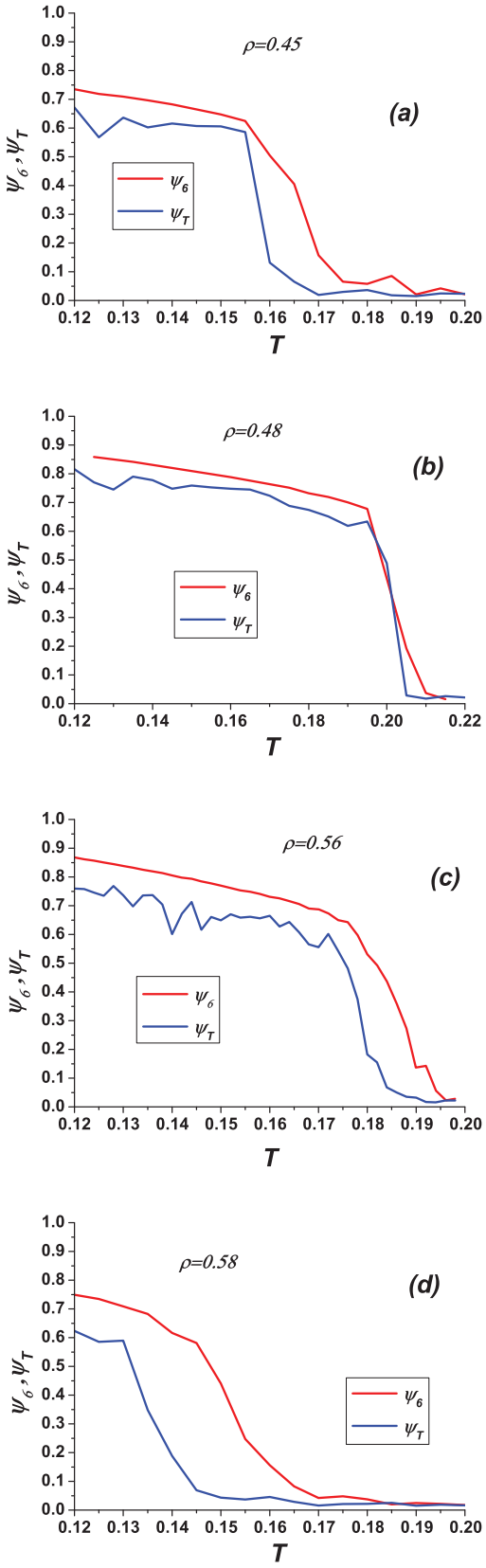

FIG. 10: (Color online) OPs ψ_T and ψ_6 as functions of temperature for $\rho = 0.45$ (a); $\rho = 0.48$ (b); $\rho = 0.56$ (c); $\rho = 0.58$. It is clearly the narrow hexatic phase in all four cases.

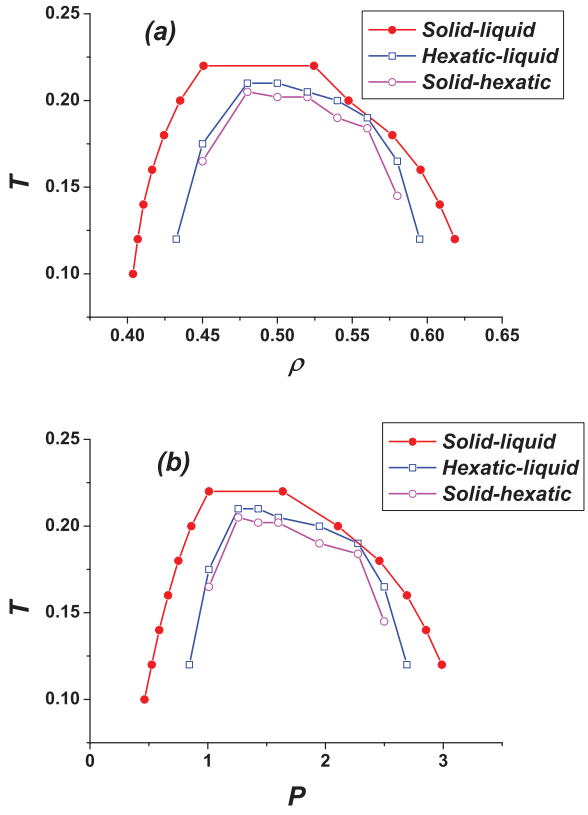

FIG. 11: (Color online) The low-density (a) and low-pressure (b) parts of the phase diagram (Fig. 3) along with the lines of solid-hexatic and hexatic-liquid transitions obtained with the help of Fig. 10. Only the upper part of the two-phase region in Fig. 3(a) is shown.

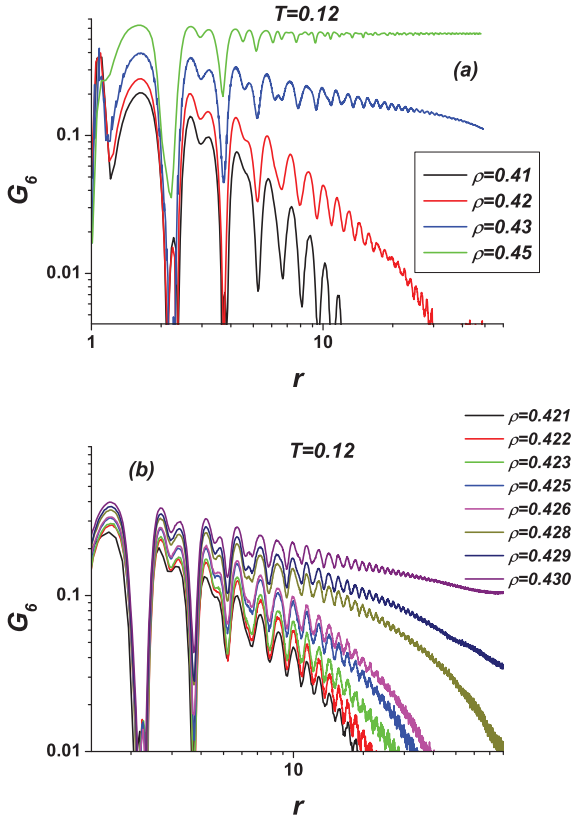

FIG. 12: (Color online) (a) Log-log plots of the orientational correlation function $G_6(r)$ at selected densities across the hexatic region for $T = 0.12$. Upon increasing ρ from 0.41 to 0.45 there is a qualitative change in the large-distance behavior of $G_6(r)$, from constant (solid) to power-law decay (hexatic fluid), up to exponential decay (normal fluid). Note that, consistently with the KTHNY theory, the decay exponent η is less than 1/4 for $\rho > 0.4325$; (b) Detailed behavior of $G_6(r)$ in the interval of densities $0.421 - 0.43$.

($\rho = 0.48$), the region of the hexatic phase is very narrow, however, we cannot conclusively determine whether the width of the hexatic phase in the maximum point is equal to zero. In Fig. 11, the phase transition lines of the solid-hexatic and hexatic-liquid transitions are shown in comparison with the solid-liquid transition line (see Fig. 3) in $\rho - T$ and $P - T$ planes. One can see that the transitions are mainly inside the solid region, obtained in the framework of the free-energy calculations. This fact also supports the idea that the melting in this region occurs through two continuous transitions. The errors in calculation of the OOP ψ_6 are less than 1%, while the errors of the translational order parameter ψ_T do not exceed 5%.

A more direct evidence of the hexatic phase emerges from the large-distance behavior of the OCF. We plot this function in Fig. 12 and Fig. 13 at various densities across the hexatic phase for $T = 0.12$ and $T = 0.16$. Calculations of the orientational correlation function are made for 102400 particles. Index η is shown as a function of density ρ for $T = 0.12$ in Fig. 14. From Fig. 14 one can see that $\eta = 1/4$ for $\rho \approx 0.4325$ and $\rho \approx 0.595$ at $T = 0.12$. These points correspond to the densities of normal fluid-hexatic transition at the phase diagram in Fig. 11(a). In principle, this approach can be applied for the construction of the phase diagram, however, it is rather time consuming and cannot give the possibility to calculate the line of the solid-hexatic transition.This behavior is consistent with the line of hexatic-normal liquid transition shown in Fig. 11(a).

It should be noted, that the scaling analysis made in accordance with the algorithm in Refs. [42, 47] also supports the melting scenario described above. For the OOP we used a system of 102400 particles which was divided in subboxes. The subbox size parameter M_b is equal to the number of subboxes along the edge of the total system and varies in our simulations from 1 to 16. As expected (see [42, 47]), the bond-orientational order parameter does not change in the ordered region while it increases with increasing the number of the subboxes in

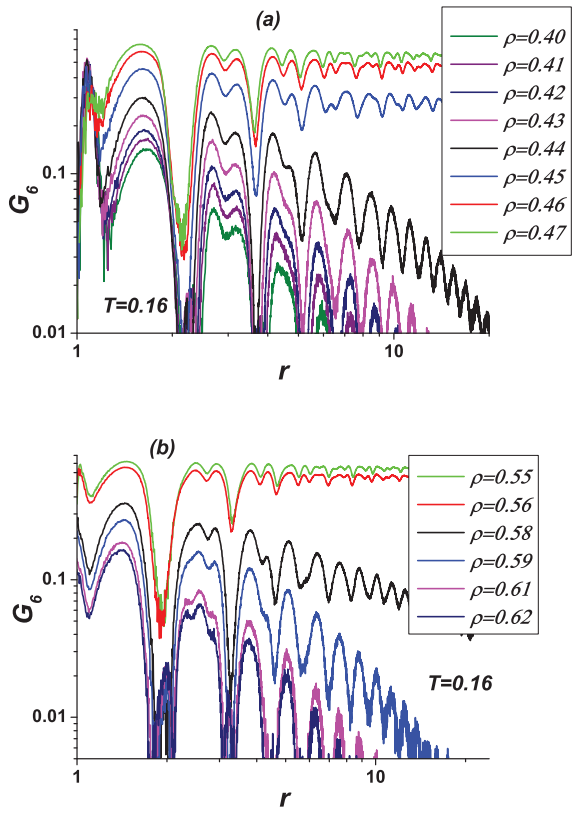

FIG. 13: (Color online) Log-log plots of the orientational correlation function $G_6(r)$ at selected densities across the hexatic region for $T = 0.16$. Upon increasing ρ from 0.40 to 0.47 (a) and from 0.55 to 0.62 there is a qualitative change in the large-distance behavior of $G_6(r)$, from constant (solid) to power-law decay (hexatic fluid), up to exponential decay (normal fluid). The behavior is consistent with the line of hexatic-normal liquid transition shown in Fig. 11(a).

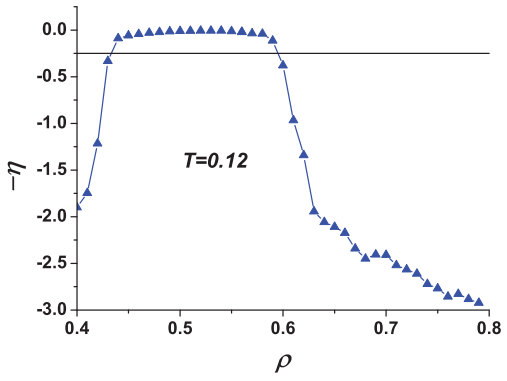

FIG. 14: (Color online) Index η as a function of density. Horizontal line corresponds to $\eta = 1/4$.

the liquid phase. At the same time, we observe an increase of OOP susceptibility without the change of the locations of the peaks maxima.

The similar analysis was made for the melting of the square lattice region of the phase diagram, and it was shown that the square lattice melts through the first-order phase transition.

CONCLUSIONS

In conclusion, we have compared the phase diagrams and anomalous behavior of two-dimensional ($2D$) and three dimensional ($3D$) classical particles repelling each other through an isotropic core-softened potential. We have provided the unambiguous evidence of the occurrence of two-stage continuous reentrant melting via a hexatic phase in the 2D core-softened model at low densities, while at high densities the melting occurs through the conventional first-order phase transition. We have validated a number of KTHNY predictions. This kind of behavior can be understood from the consideration of the potential (1). It is widely believed that the 2D melting transition scenario corresponds to the KTHNY one for the softer potentials, however, the systems with hard potentials melt through first-order transition. The behavior of the system described by the potential (1) is determined by the soft long-range part of the potential at low densities. At the same time, the hard core of the potential plays the main role at the high densities. It seems that this is the reason of the observed peculiarities of the phase diagram. The present discovery of reentrant-hexatic behavior in the core-softened potential is relevant for many soft-matter systems. For instance, one can engineer colloidal particles interacting through a temperature modulated softened repulsion, which will likely exhibit reentrant melting in a range of packing fractions well below the density at which hard-core crystallization occurs.

It was also shown, that the order of the region of anomalous diffusion and the region of structural anomaly is inverted in comparison with the $3D$ case, where the order of the anomalies is waterlike, and has the silicalike sequence. This fact shows that the dynamics of $2D$ liquids is really different from the dynamics of the corresponding $3D$ system. The reasons for this kind of behavior can be twofold. First of all, confining the system in $2D$ changes the geometry of the spatial distribution of the constituent molecules and the ways by which those molecules can dynamically rearrange. Second, the density fluctuations in $2D$ are much higher than in $3D$. As it was discussed above, these fluctuations lead to the change of the melting scenario from the first order one to two continuous transitions. It seems that the fluctuations can drastically change the diffusivity in the system, but do not affect considerably the structural and density anomalies.

These results may be also useful for the qualitative understanding the behavior of confined monolayers of charge-stabilized colloids with a softened core and water confined between two hydrophobic plates [1, 2, 54–57].

ACKNOWLEDGMENTS

We are greateful to S. M. Stishov, V. V. Brazhkin, and E.E. Tareyeva for stimulating discussions. Yu.F. and E.T. also thank the Russian Scientific Center Kurchatov Institute and Joint Supercomputing Center of the Russian Academy of Science for computational facilities. The work was supported in part by the Russian Foundation for Basic Research (Grants No 14-02-00451, 13-02-91177, 13-02-12008, 13-02-00579, and 13-02-00913) and the Ministry of Education and Science of Russian Federation (project MK-2099.2013.2).

[1] M. Alcoutlabi and G. B. McKenna, J. Phys.: Condens. Matter **17**, R461 (2005).
[2] S.A. Rice, Chem. Phys. Lett. **479**, 1 (2009).
[3] Y.D. Fomin, N.V. Gribova, V.N. Ryzhov, S.M Stishov, and D. Frenkel, J. Chem. Phys. **129**, 064512 (2008).
[4] N.V. Gribova, Y.D. Fomin, D. Frenkel, and V.N. Ryzhov, Phys. Rev. E **79** 051202 (2009).
[5] Y.D. Fomin, E.N. Tsiok, and V.N. Ryzhov, J. Chem. Phys. **135**, 234502 (2011).
[6] Y.D. Fomin, E.N. Tsiok, and V.N. Ryzhov, European Physical Journal - Special Topics **216**, 165 (2013).
[7] R.E. Ryltsev, N.M. Chtchelkatchev, and V.N. Ryzhov, Phys. Rev. Lett. **110**, 025701 (2013).
[8] Y.D. Fomin, E.N. Tsiok, and V.N. Ryzhov, Phys. Rev. E **87**, 042122 (2013).
[9] S.V. Buldyrev, G. Malescio, C.A. Angell, N. Giovambattista, S. Prestipino, F. Saija, H.E. Stanley, and L. Xu, J. Phys.: Condens. Matter **21**, 504106 (2009).
[10] P. Vilaseca and G. Franzese, Journal of Non-Crystalline Solids **357**, 419 (2011).
[11] G. Franzese, J. Mol. Liq. **136**, 267 (2007).
[12] P. Vilaseca and G. Franzese, J. Chem. Phys. **133**, 084507 (2010).
[13] J. A. Abraham, S. V. Buldyrev, and N. Giovambattista, J. Phys. Chem. B **115**, 14229 (2011).
[14] A. B. de Oliveira, P. A. Netz, T. Colla, and M. C. Barbosa, J. Chem. Phys. **125**, 124503 (2006).
[15] A. B. de Oliveira, P. A. Netz, and M. C. Barbosa, Europhys. Lett. **85**, 36001 (2009).
[16] S. Prestipino, F. Saija, and P.V. Giaquinta, J. Chem. Phys. **137**, 104503 (2012).
[17] S. Prestipino, F. Saija, and G. Malescio, J. Chem. Phys. **133**, 144504 (2010).
[18] C.A. Angell, E.D. Finch, and P. Bach, J. Chem. Phys. **65**, 3063 (1976).
[19] J. R. Errington and P. G. Debenedetti, Nature (London) **409**, 318 (2001).
[20] P.A. Netz, F.V. Starr, H.E. Stanley, and M.C. Barbosa, J. Chem. Phys. **115**, 344 (2001).
[21] L. Xu, P. Kumar, S. V. Buldyrev, S.-H. Chen, P. H. Poole, F. Sciortino, and H. E. Stanley, Proc. Natl. Acad. Sci. USA **102**, 16558 (2005).
[22] V.V. Brazhkin, Yu.D. Fomin, A.G. Lyapin, V.N. Ryzhov, and E.N. Tsiok, J. Phys. Chem. B **115**, 14112 (2011).
[23] V.V. Brazhkin and V.N. Ryzhov, J. Chem. Phys. **135**, 084503 (2011).
[24] J. Luo, L. Xu, Y.E. Stanley, and S.V. Buldyrev, Phys. Rev. Lett. **112**, 135701 (2014).
[25] M.S. Shell, P.G. Debenedetti, A.Z. Panagiotopoulos, Phys. Rev. E **66**, 011202 (2002).
[26] V.N. Ryzhov and E.E. Tareyeva, Phys. Rev. B **51** 8789 (1995).
[27] V.N. Ryzhov and E.E. Tareyeva, Zh. Eksp. Teor. Fiz. **108**, 2044 (1995) [JETP **81**, 1115 (1995)].
[28] V.N. Ryzhov and E.E. Tareyeva, Physica A **314**, 396 (2002).
[29] V.N. Ryzhov and E.E. Tareyeva, Theor. Math. Phys. **130**, 101 (2002)(DOI: 10.1023/A:1013884616321)
[30] B.I. Halperin and D.R.Nelson, Phys. Rev. Lett. **41** 121 (1978); D.R.Nelson and B.I. Halperin, Phys. Rev. B **19** 2457 (1979); A.P. Young, Phys. Rev. B **19** 1855 (1979).
[31] M. Kosterlitz and D.J. Thouless, J. Phys. C **6** 1181 (1973).
[32] C.C. Grimes and G. Adams, Phys. Rev. Lett. **42**, 795 (1979).
[33] K.J. Strandburg, Rev. Mod. Phys. **60**, 161 (1988).
[34] Urs Gasser, C. Eisenmann, G. Maret, and P. Keim, ChemPhysChem **11**, 963 (2010).
[35] K. Zahn and G. Maret, Phys. Rev. Lett. **85** 3656 (2000).
[36] P. Keim, G. Maret, and H.H. von Grunberg, Phys. Rev. E **75**, 031402 (2007).
[37] S.T. Chui, Phys. Rev. B **28**, 178 (1983).
[38] W. Janke and H. Kleinert, Phys. Rev. B **41**, 6848 (1990).
[39] V.N. Ryzhov, Theor. Math. Phys. **88**, 990 (1991) (DOI: 10.1007/BF01027701).
[40] V.N. Ryzhov, Zh. Eksp. Teor. Fiz. **100**, 1627 (1991) [Sov. Phys. JETP **73**, 899 (1991)].
[41] J. Lee and K.J. Strandburg, Phys. Rev. B **46**, 11190 (1992).
[42] H. Weber, D. Marx, and K. Binder, Phys. Rev. B **51**, 14636 (1995).
[43] C.H. Mak, Phys. Rev. E **73**, 065104 (2006).
[44] A. Jaster, Europhys. Lett., **42**, 277 (1998).
[45] K. Bagchi, H.C. Andersen, and W. Swope, Phys. Rev. Lett. **76**, 255 (1996).
[46] E.P. Bernard and W. Krauth, Phys. Rev. Lett. **107**, 155704 (2011); M. Engel, J.A. Anderson, S.C. Glotzer, M. Isobe, E.P. Bernard, and W. Krauth, Phys. Rev. E **87**, 042134 (2013).
[47] K. Binder, S. Sengupta, and P. Nielaba, J. Phys.: Condens. Matter **14**, 2323 (2002).
[48] P. Bladon and D. Frenkel, Phys. Rev. Lett. **74**, 2519 (1995).
[49] S.I. Lee and S.J. Lee, Phys. Rev. E **78**, 041504 (2008).
[50] S. Prestipino, F. Saija, and P.V. Giaquinta, Phys. Rev. Lett. **106**, 235701 (2011).
[51] Frenkel Daan and Smit Berend, *Understanding molecular simulation (From Algorithms to Applications), 2nd Edition* (Academic Press, 2002).
[52] http://lammps.sandia.gov/
[53] M.R. Sadr-Lahijany, A. Scala, S.V. Buldyrev, H.E. Stanley, Phys. Rev. Lett. **81**, 4895 (1998).
[54] L.B. Krott and M.C. Barbosa, J. Chem. Phys., **138**

084505 (2013).
[55] A.M. Almudallal, S.V. Buldyrev, and I. Saika-Voivod, J. Chem. Phys., **137** 034507 (2012).
[56] L.B. Krott and J.R. Bordinb, J. Chem. Phys. **139**, 154502 (2013).
[57] L. B. Krott and M. C. Barbosa, Phys. Rev. E **89**, 012110 (2014).